Selective photocatalytic reduction of CO_2 to methanol in CuO-loaded $NaTaO_3$ nanocubes in isopropanol

Tianyu Xiang[1,2], Feng Xin[*,1,2,§], Jingshuai Chen[1,2], Yuwen Wang[1,2], Xiaohong Yin[3] and Xiao Shao[3]

Abstract

A series of $NaTaO_3$ photocatalysts were prepared with Ta_2O_5 and NaOH via a hydrothermal method. CuO was loaded onto the surface of $NaTaO_3$ as a cocatalyst by successive impregnation and calcination. The obtained photocatalysts were characterized by XRD, SEM, UV–vis, EDS and XPS and used to photocatalytically reduce CO_2 in isopropanol. This worked to both absorb CO_2 and as a sacrificial reagent to harvest CO_2 and donate electrons. Methanol and acetone were generated as the reduction product of CO_2 and the oxidation product of isopropanol, respectively. $NaTaO_3$ nanocubes loaded with 2 wt % CuO and synthesized in 2 mol/L NaOH solution showed the best activity. The methanol and acetone yields were 137.48 μmol/(g·h) and 335.93 μmol/(g·h), respectively, after 6 h of irradiation. Such high activity could be attributed to the good crystallinity, morphology and proper amount of CuO loading, which functioned as reductive sites for selective formation of methanol. The reaction mechanism was also proposed and explained by band theory.

Introduction

Global warming is one of the most major environmental problems that we are facing in the 21st century [1]. Carbon dioxide (CO_2) contributes significantly to global climate change as it is the main greenhouse gas present in the atmosphere and primarily formed from the consumption of fossil fuels [2]. To date, many methods have been proposed to reduce the emitted CO_2 concentration. A particularly advantageous approach is the capture of CO_2 from the atmosphere for the conversion to fuel by using a sustainable source of energy like sunlight. In this way, global warming and energy shortage problems can be solved simultaneously [3-7]. For this purpose, the photocatalytic conversion of CO_2 to fuel is particularly emphasized.

In 1979, Inoue et al. [8] first reported the photocatalytic reduction of CO_2 in aqueous solution using several semiconductor materials (WO_3, TiO_2, ZnO, CdS, GaP and SiC), producing

CH_3OH, HCOOH, HCHO and trace amounts of CH_4. In the 1990s, Ta oxide photocatalysts began to draw attention in the field of water splitting. A series of Ta catalysts, such as $LiTaO_3$ [9], $NaTaO_3$ [10], $KTaO_3$ [11], $AgTaO_3$ [12], $CaTa_2O_6$ [13], $SrTa_2O_6$ [13], $KBa_2Ta_3O_{10}$ [14], were proved to efficiently split water. In the 21st century, the study of Ta catalysts for the reduction of CO_2 began. Kentaro Teramura et al. [15] prepared $ATaO_3$ (A = Li, Na, K) compounds using a solid state reaction (SSR) method to reduce CO_2 in the presence of H_2. The only product was CO and the order of photocatalytic activity was $LiTaO_3 > NaTaO_3 > KTaO_3$, which was consistent with that of the E_g (band gap) values. However, the highest yield of CO in $LiTaO_3$ was 0.42 μmol/g after 24 h of photoirradiation, which was still far from satisfactory. Ye et al. [16] synthesized a series of noble-metal-loaded $NaTaO_3$ samples to reduce CO_2 with water. H_2 was introduced into this process as an electron donor. $Ru/NaTaO_3$ was found to have the best activity (CH_4 51.8 μmol/(g·h)) and product selectivity in converting CO_2 to CH_4. Junwang Tang and his team [17] prepared $KTaO_3$ nanoflakes by a solvothermal method in a hexane–water mixture and reduced CO_2 using pure water as an electron donor. The activity was quite high for both H_2 and CO production, achieving 20× (H_2) and 7× (CO) higher than that of the cubic sample prepared by the solid state reaction. This was an indication that the catalyst morphology played a crucial role in activity. Jeffrey C. S. Wu et al. [18] prepared NiO-loaded $InTaO_4$ photocatalysts by a sol–gel method and carried out the photocatalytic reduction of CO_2 in a self-made optical fiber reactor filled with 0.2 mol/L NaOH solution. The formation rate of methanol was 11.1 μmol/(g·h) under halogen lamp irradiation at 25 °C. Ru-Shi Liu and co-workers [19] prepared a series of nanostructured core–shell materials (Ni@NiO/N-doped $InTaO_4$ photocatalysts) for the reduction of CO_2 to methanol in pure water. In these structures, the core–shell nanostructure might offer a new reaction center transferred from the surface of the $InTaO_4$ material.

In this paper, we report the photocatalytic reduction of CO_2 to methanol using CuO-loaded $NaTaO_3$ catalysts. $NaTaO_3$ nanocubes were synthesized via a hydrothermal method using Ta_2O_5 and NaOH. CuO was loaded onto the surface of $NaTaO_3$ by impregnation, where CuO acts as a cocatalyst for CO_2 reduction, promoting charge transfer and limiting the fast recombination of electrons and holes [20,21]. According to the literature, Cu oxides and Cu cations are active cocatalysts for CO_2 reduction and could serve as reductive sites for selective reduction of CO_2 to methanol [22-27]. Isopropanol was employed as both an absorber and a sacrificial reagent due to its good capability to absorb CO_2 and donate electrons [28-30]. Acetone, an important industrial material, was generated as the oxidation product of isopropanol.

Experimental
Catalyst preparation
Tantalum oxide (Ta_2O_5, 99.99%), sodium hydroxide (NaOH, 96%) and isopropanol (iPrOH, 99.9%) were purchased from Aladdin Industrial Corporation. Copper nitrate ($Cu(NO_3)_2·3H_2O$, AR) was purchased from Tianjin Guangfu Chemical Reagent Company. All reagents were used as received without any further purification.

The $NaTaO_3$ nanocubes were synthesized by a hydrothermal method as reported by Li et al. [31]. In a typical procedure, 0.442 g of Ta_2O_5 and a sufficient amount of NaOH were added into a Teflon-lined autoclave with a total volume of 50 mL, and deionized water was filled up to 40 mL. The autoclave temperature was held at 140 °C for 12 h then cooled to room temperature in air. The obtained product was washed with deionized water several times before being dried at 80 °C in an oven overnight. The as-prepared catalysts were denoted as 1M-$NaTaO_3$, 2M-$NaTaO_3$, 3M-$NaTaO_3$, 4M-$NaTaO_3$, corresponding to a NaOH concentration of 1 mol/L, 2 mol/L, 3 mol/L, 4 mol/L, respectively.

CuO was loaded onto the surface of $NaTaO_3$ by impregnation. 0.1 g of 2M-$NaTaO_3$ and a given amount of $Cu(NO_3)_2·3H_2O$ were mixed in a crucible with 3 mL deionized water. After stirring for 10 min, the crucible was transferred into a muffle furnace and held for 4 h at 450 °C. After cooling down to room temperature, the resulting product was washed and dried at 80 °C overnight. The as-prepared CuO–$NaTaO_3$ catalysts were denoted as 1wt-$NaTaO_3$, 2wt-$NaTaO_3$, 3wt-$NaTaO_3$, 4wt-$NaTaO_3$ and 5wt-$NaTaO_3$ corresponding to 1 wt %, 2 wt %, 3 wt %, 4 wt % and 5 wt % CuO loading on $NaTaO_3$, respectively.

Catalyst characterization
The catalysts were characterized by X-ray diffraction (XRD, Bruke/D8-Advance, Cu Kα radiation, λ = 0.154056 nm) at a scanning rate of 4°/min ranging from 15° to 70°. The morphology was observed with a Hitachi S-4800 field emission scanning electron microscope (SEM) with an accelerating voltage of 3.0 kV. The surface composition of the catalysts was investigated using a Thermo Scientific energy dispersion X-ray (EDX) fluorescence analyzer (with a Mg Kα ADES (hv = 1253.6 eV) source) as an addition to the SEM and XPS (PHA-5400, SPECS, America). Light absorbance was measured with a Shimadzu UV-2550 spectrometer using $BaSO_4$ as a reference in the wavelength region of 190–600 nm.

Photocatalytic reaction
The photocatalytic reduction of carbon dioxide was carried out in a transparent batch reactor with a slurry bed with cooling

jacket. The light source was a 250 W high-pressure mercury lamp with an irradiation peak at about 365 nm. The reaction temperature was controlled by a thermostatic water bath at 25 ± 3 °C. The reactor, in which 12 mg of catalyst was dispersed in 12 mL of isopropanol, was tightly sealed during the reaction. A magnetic stirrer agitated at the bottom of the suspension until the reaction ended. Before irradiation, CO_2 (99.99% purity) was bubbled through the reactor for 30 min to eliminate air and saturate the suspension. A typical run was 6 h.

After reaction, the suspension was centrifuged and the liquid sample was examined by a GC-MS (Agilent 5975C) and quantified by a GC (Agilent 7890A, FID, HP-WAX 60 m column). Control experiments were also carried out to confirm that methanol generation was complete in the CO_2 reduction. Neither methanol nor acetone was detected in dark or in the absence of catalyst. When N_2 was bubbled into the reactor instead of CO_2, only acetone was found after the reaction, indicating the likelihood that the isopropanol was oxidized to acetone.

Results and Discussions
Catalyst characterization

Figure 1 shows the XRD patterns of $NaTaO_3$ nanocubes prepared with different NaOH concentrations. All diffraction peaks can be indexed to the orthorhombic phase $NaTaO_3$ structure according to JCPDS#25-0836 with the space group belonging to

Figure 1: XRD patterns of $NaTaO_3$ nanocubes.
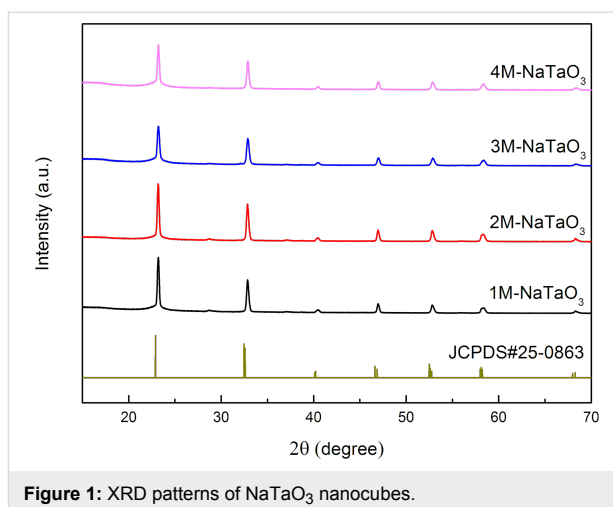
I, and lattice parameters $a = 5.513$ Å, $b = 7.750$ Å, and $c = 5.494$ Å. As Ta_2O_5 could not completely convert to $NaTaO_3$ under conditions of low NaOH concentration during the hydrothermal treatment [32,33], sufficient NaOH was used to ensure that pure $NaTaO_3$ was obtained. As calculated by Jade 5.0 software, all the samples had good crystallinity (>98%), which was attributed to the hydrothermal method of catalyst preparation.

Figure 2 shows the SEM images of $NaTaO_3$ nanocubes synthesized with different NaOH concentrations. When the NaOH
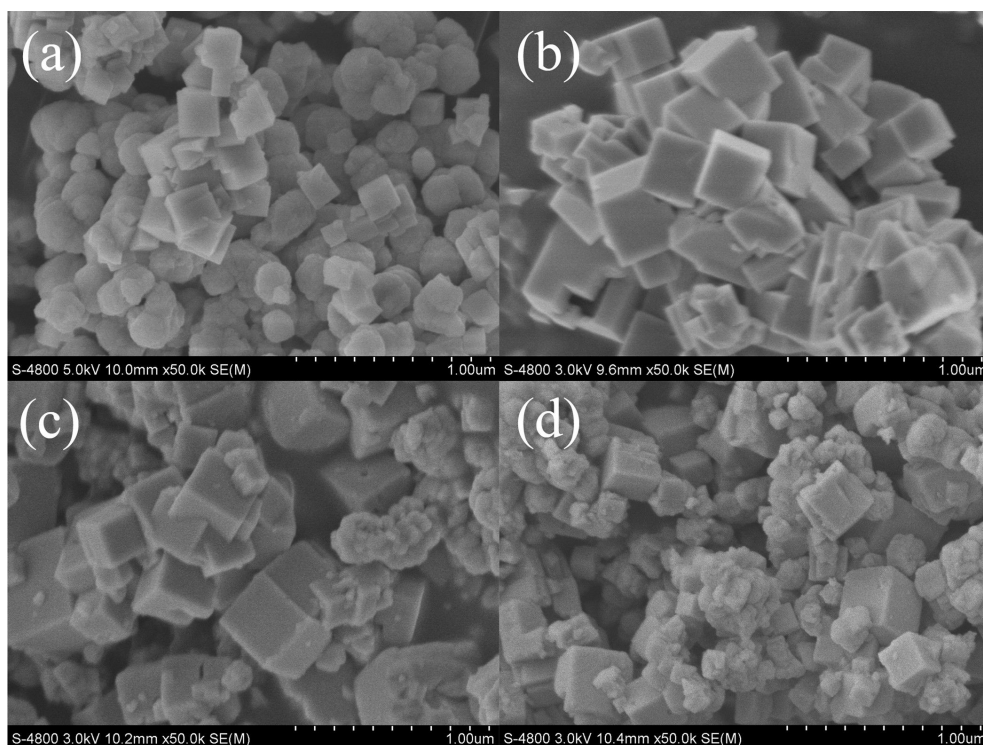

Figure 2: SEM images of $NaTaO_3$ nanocubes: (a) 1M-$NaTaO_3$, (b) 2M-$NaTaO_3$, (c) 3M-$NaTaO_3$, and (d) 4M-$NaTaO_3$.

concentration was 1 mol/L, only a small percentage of the NaTaO$_3$ grew into cubes. As the NaOH concentration was increased to 2 mol/L, almost all of the particles became larger cubes with an average size of about 300 nm. When the NaOH concentration was increased to 3 mol/L and 4 mol/L, the ideal morphology of the nanocubes was disrupted and fewer nanocubes were observed. Generally, the SEM image of 2M-NaTaO$_3$ presents the best morphology. He et al. [34] reported a hydrothermal synthesis of NaTaO$_3$ with Ta$_2$O$_5$ powder and NaOH followed a dissolution–precipitation mechanism, where the concentration of the NaOH solution played a crucial role on the morphology of the crystal. This was confirmed in our work.

Figure 3 shows UV–vis diffuse reflectance spectra and optical absorption edges of NaTaO$_3$ nanocubes prepared with different concentrations of NaOH. From Figure 3a, it can be observed that the main absorption peaks are around 300 nm, which means the powders have an apparent absorption of UV light. The band gap energy (E_g) of each catalyst, prepared with different NaOH concentrations from 1 mol/L to 4 mol/L, can be seen in Figure 3b where the E_g values of these NaTaO$_3$ samples range from 4.06 to 4.12 eV.

Figure 4 shows XRD patterns of 2M-NaTaO$_3$ nanocubes loaded with different amounts of CuO. Comparing with a pure NaTaO$_3$ catalyst, the XRD patterns of the CuO-loaded materials seemed not to change, indicating that the crystalline phase of NaTaO$_3$ was not affected by CuO loading. CuO was also not detected because the loading amount was relatively low [35].

SEM images of CuO–NaTaO$_3$ nanocubes are shown in Figure 5. It can be seen that the surface of pure NaTaO$_3$ nanocubes was flat and smooth (Figure 5a). With moderate

Figure 4: XRD patterns of 2M-NaTaO$_3$ nanocubes loaded with different amounts of CuO.
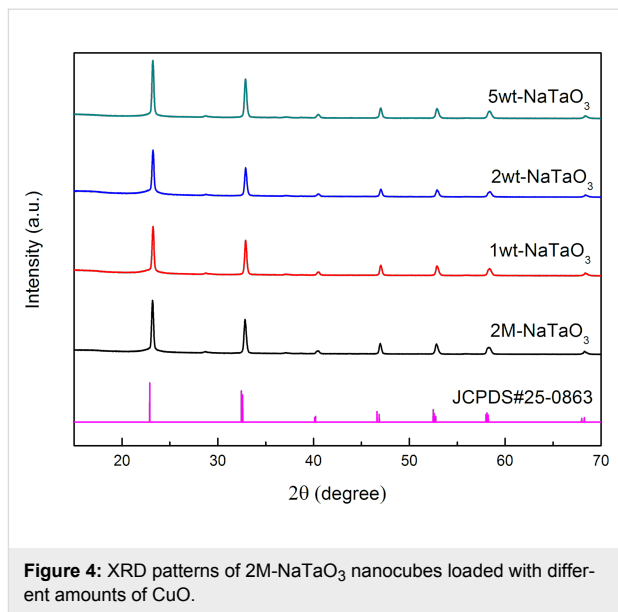
loadings of 1 wt % and 2 wt % CuO, CuO particles were dispersed on the surface of the NaTaO$_3$ nanocubes with an average size of tens of nanometers (Figure 5b and Figure 5c). When the loading reached 5 wt %, the CuO nanoparticles began to aggregate and large clusters were formed (Figure 5d).

The UV–vis diffuse reflectance spectra of CuO–NaTaO$_3$ are shown in Figure 6. With a large energy gap, it can be found that pure NaTaO$_3$ had low light absorbance in the visible region. After CuO was loaded, the absorbance of the CuO–NaTaO$_3$ catalysts in the visible light region ($\lambda > 400$ nm) became much stronger with the increase of CuO loading. The increase in visible light absorbance correlates with the formation rate and increase in electrons and holes on the photocatalyst surface [35].
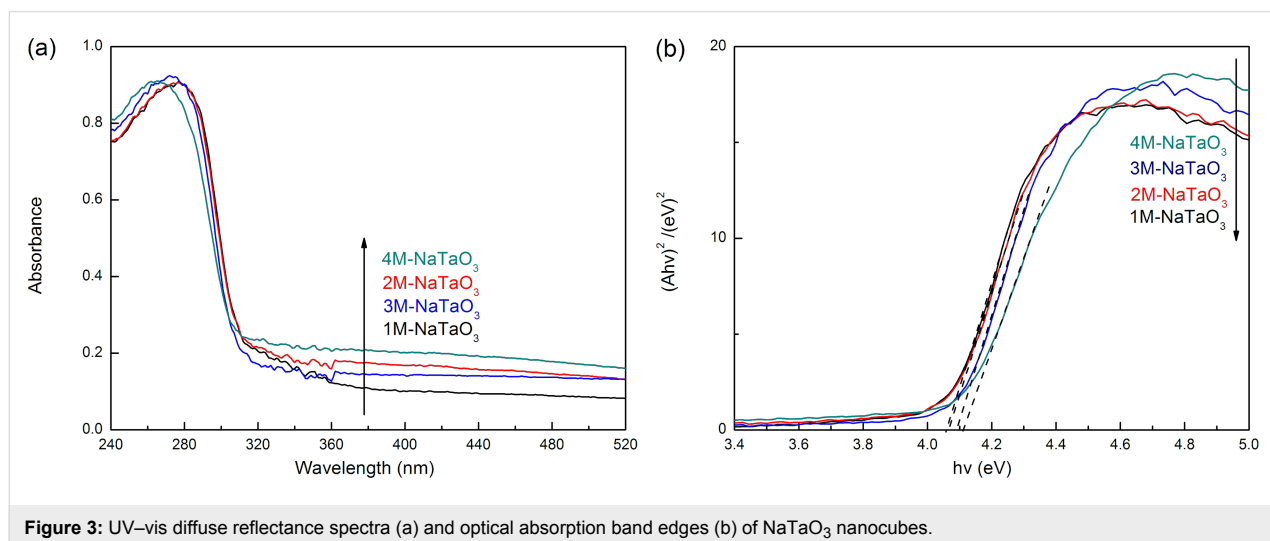

Figure 3: UV–vis diffuse reflectance spectra (a) and optical absorption band edges (b) of NaTaO$_3$ nanocubes.
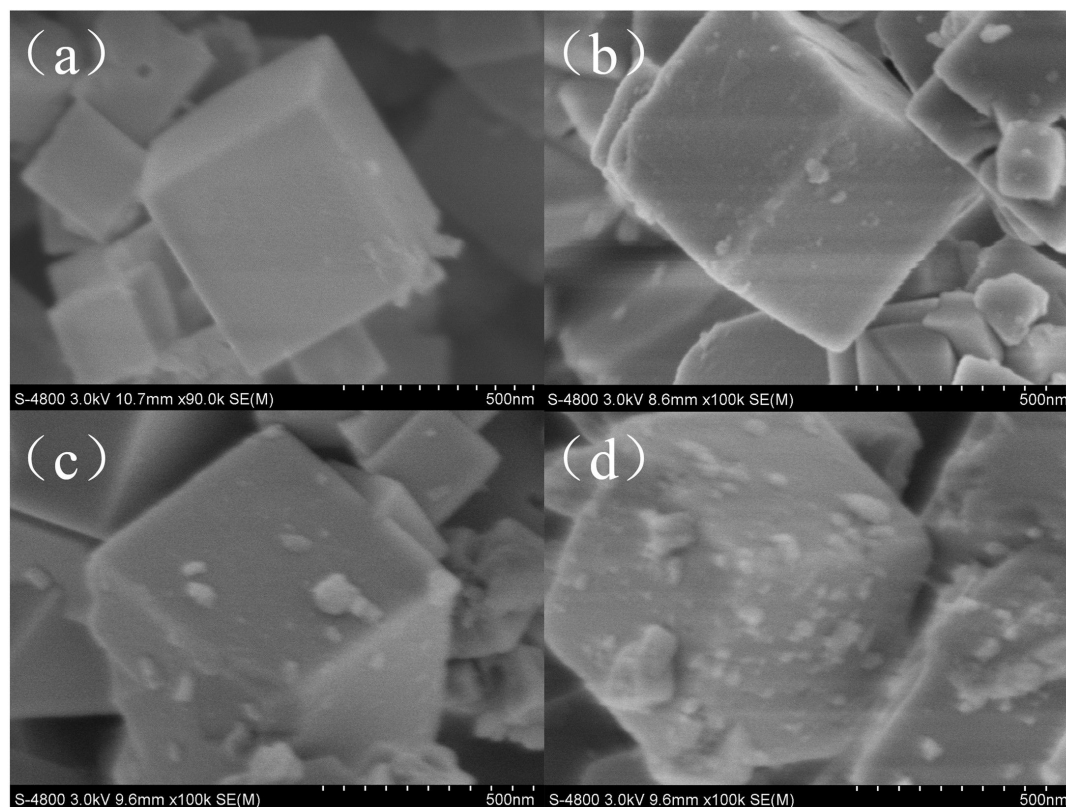
Figure 5: SEM images of CuO–NaTaO$_3$ nanocubes: (a) 2M-NaTaO$_3$, (b) 1wt-NaTaO$_3$, (c) 2wt-NaTaO$_3$, and (d) 5wt-NaTaO$_3$.
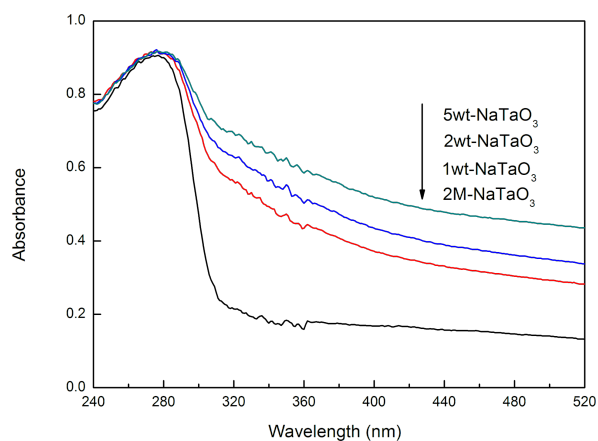

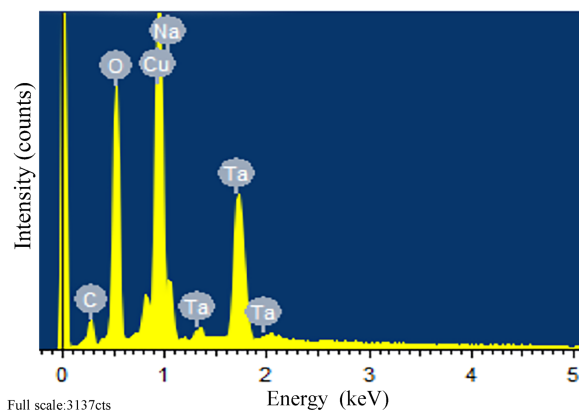**Figure 6:** UV–vis diffuse reflectance spectra of CuO-loaded 2M-NaTaO$_3$ nanocubes.

Figure 7: EDS spectrum of 5wt-NaTaO$_3$.

Energy-dispersive X-ray spectroscopy (EDS) and X-ray photoelectron spectroscopy (XPS) were carried out to confirm that CuO was loaded onto the surface of NaTaO$_3$ nanocubes. Figure 7 presents the EDS analysis of 5wt-NaTaO$_3$, which was performed over a single nanoparticle on the catalyst surface. It can be seen that the main compositional elements of the nanoparticle were Cu and O. Figure 8 demonstrates the Cu 2p XPS peak of 2M-NaTaO$_3$, 2wt-NaTaO$_3$ and 5wt-NaTaO$_3$. The two peaks located at 933.20 eV and 953.20 eV corresponded to Cu 2p$_{3/2}$ and Cu 2p$_{1/2}$ and a satellite peak was also observed at about 944 eV. These peaks were characteristic for Cu^{2+}, which indicated that Cu existed in the form of CuO [36-39]. The peak intensity increases with increasing loading.

Figure 8: Smoothed Cu 2p XPS peaks 2M-NaTaO$_3$, 2wt-NaTaO$_3$ and 5wt-NaTaO$_3$.
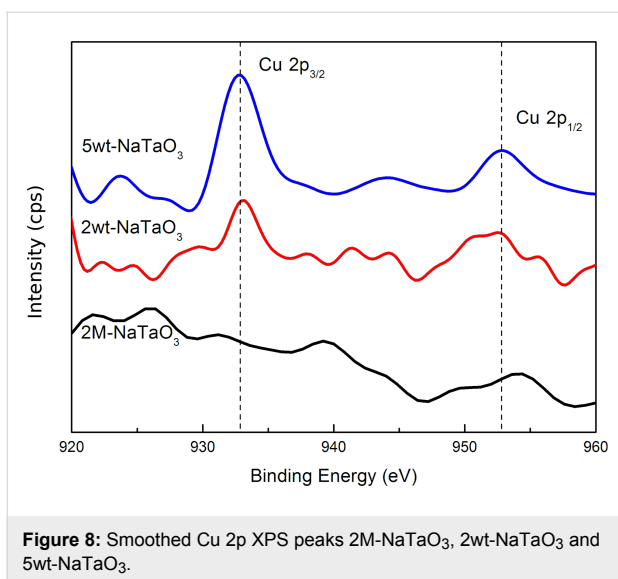
Photocatalytic reduction of CO$_2$

The photocatalytic activity of CuO–NaTaO$_3$ samples was evaluated by photocatalytic reduction of CO$_2$ in isopropanol under UV light irradiation for 6 h. Methanol and acetone were generated as the reduction product of CO$_2$ and the oxidation product of isopropanol, respectively. 2M-NaTaO$_3$ was chosen for CuO loading because of its good morphology. In our experiments, there was no methanol generation in the absence of copper, which was consistent with Hirato's report [40].

Figure 9 represents the methanol and acetone yield for 2M-NaTaO$_3$ loaded with different amounts of CuO after 6 h of irradiation. CuO nanoparticles loaded on the surface of 2M-NaTaO$_3$ functioned as reductive sites on which CO$_2$ was reduced to methanol. Below the optimal amount of CuO

Figure 9: Methanol and acetone yields for 2M-NaTaO$_3$ loaded with different amounts of CuO after 6 h of irradiation.
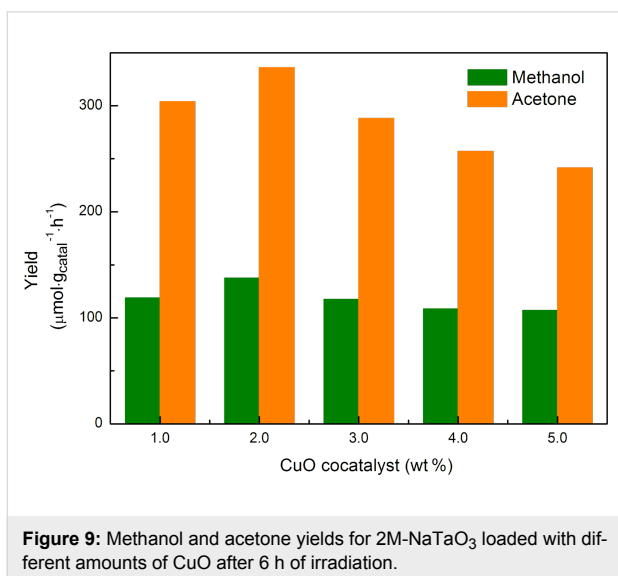
(2 wt %), the activity was promoted with the increase of CuO loading. When the loading was greater than 2 wt %, the activity began to decrease.

In our experiments, 2 wt % CuO loaded 2M-NaTaO$_3$ showed the highest activity, which was attributed to its good crystallinity, morphology and proper amount of CuO loading. According to the XRD results of non-loaded NaTaO$_3$, all samples had good crystallinity, which was beneficial to photocatalytic activity. The high crystalline quality correlates to a low number of defects. The defects usually function as recombination centers where photogenerated electrons and holes recombine fast, resulting in poor photocatalytic activity [41]. Among these catalysts, 2M-NaTaO$_3$ had the best morphology, which played a crucial role in this case. A regular morphology is helpful to the electron transmission process, as it shortens the pathway through which generated electrons transfer from the bulk to the surface of the crystal, thus making the electrons more efficient for the reaction. The CuO loading amount was another important factor. Below the optimal amount of CuO (2 wt %), the activity increased with the increase of CuO loading. For CuO loading greater than 2 wt %, the activity decreased with increasing CuO loading. An explanation for this is that the CuO nanoparticles provide more reductive sites and could reduce the recombination of photogenerated electron–hole pairs with an increase in (moderate) loading, as shown in Figure 5b and Figure 5c [42]. When excessive CuO was loaded, the CuO nanoparticles aggregated to form larger ones (shown in Figure 5d), which decreases the number of effective reductive sites. On the other hand, the large CuO particles could also decrease the efficient separation of electron–hole pairs as compared with smaller ones. Both of these situations could lead to a poor activity.

Reaction mechanism

The mechanism for photocatalytic reduction of CO$_2$ to methanol in isopropanol is shown in Figure 10. When the CuO–NaTaO$_3$ catalysts were irradiated by UV light, photogenerated electron–hole pairs were created. The electrons in the conduction band (CB) of NaTaO$_3$ (E_{CB} = −0.92 V vs NHE at pH 7, the same below) [41] could recombine with holes in the valence band (VB) of CuO, enhancing the separation and prolonging the lifespan of photogenerated electron–hole pairs. It was believed that the reduction reaction happened in the CB of CuO (−0.78 V) [35], where CO$_2$ reacted with electrons and protons to generate methanol ($E_{CO2/CH3OH}$ = −0.38 V) [43], as no methanol was detected using pure NaTaO$_3$. The valence band (VB) potential of NaTaO$_3$ is 3.13 V, which is more positive than the potential of isopropanol oxidation to acetone (about 0.47 V) [44,45], thus the oxidation reaction could happen in the VB of NaTaO$_3$.

The reaction in the CB of CuO was as follows:

$$CO_2 + 6H^+ + 6e^- = CH_3OH + H_2O$$
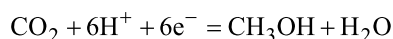
The isopropanol was oxidized into acetone and protons by holes in the valence band of $NaTaO_3$, which was illustrated by G. R. Dey [46]:

$$h^+ + (CH_3)_2 CHOH \rightarrow (CH_3)_2 C\cdot OH + H^+$$
$$2(CH_3)_2 C\cdot OH \rightarrow (CH_3)_2 CO + (CH_3)_2 CHOH$$
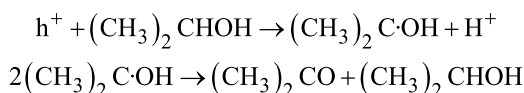
and the overall reaction was

$$CO_2 + 3(CH_3)_2 CHOH = CH_3OH + 3(CH_3)_2 CO + H_2O$$
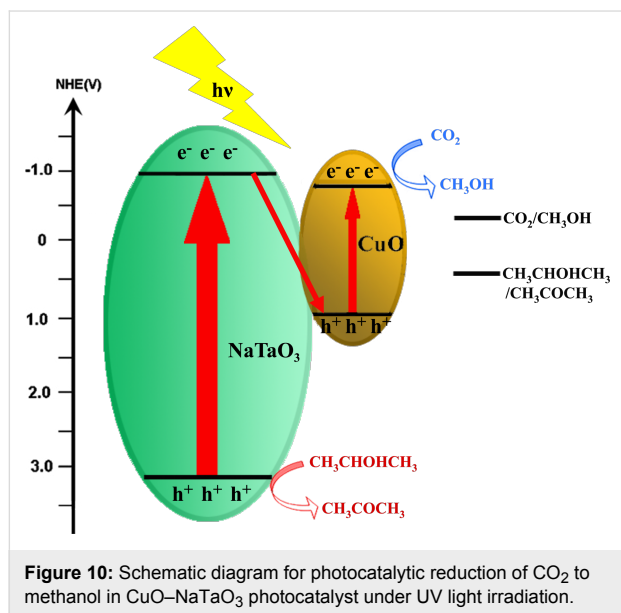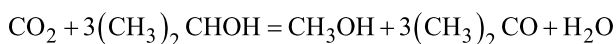

Figure 10: Schematic diagram for photocatalytic reduction of CO_2 to methanol in CuO–$NaTaO_3$ photocatalyst under UV light irradiation.

Theoretically, one mole of methanol and three moles of acetone were generated simultaneously. But in our experiments, the mole ratio of acetone to methanol ranged from 2.33 to 2.55. This was attributed to the generation of acetone that was sequentially oxidized into small molecules, which were not detectable by GC.

Conclusion

$NaTaO_3$ nanocubes were synthesized with Ta_2O_5 powder and NaOH solution via a hydrothermal method. CuO was loaded onto the surface of $NaTaO_3$ by impregnation to suppress the electron–hole recombination and functioned as a reductive site for methanol formation. Acetone was also generated as the oxidation product of isopropanol. With 2 wt % CuO loading, $NaTaO_3$ prepared by 2 mol/L NaOH solution showed the best performance. The highest yields of methanol and acetone were

137.48 μmol/(g·h) and 335.93 μmol/(g·h), respectively, after 6 h of irradiation. These good yields were attributed to the good crystallinity and morphology of $NaTaO_3$ and the proper loading amount of CuO on $NaTaO_3$. The mechanism for photocatalytic reduction of CO_2 in isopropanol to methanol was also proposed and explained by band theory.

References

1. Roy, S. C.; Varghese, O. K.; Paulose, M.; Grimes, C. A. *ACS Nano* **2010,** *4,* 1259–1278. doi:10.1021/nn9015423
2. Izumi, Y. *Coord. Chem. Rev.* **2013,** *257,* 171–186. doi:10.1016/j.ccr.2012.04.018
3. Ahmed, N.; Shibata, Y.; Taniguchi, T.; Izumi, Y. *J. Catal.* **2011,** *279,* 123–135. doi:10.1016/j.jcat.2011.01.004
4. Ahmed, N.; Morikawa, M.; Izumi, Y. *Catal. Today* **2012,** *185,* 263–269. doi:10.1016/j.cattod.2011.08.010
5. Kubacka, A.; Fernández-García, M.; Colón, G. *Chem. Rev.* **2012,** *112,* 1555–1614. doi:10.1021/cr100454n
6. Morris, A. J.; Meyer, G. J.; Fujita, E. *Acc. Chem. Res.* **2009,** *42,* 1983–1994. doi:10.1021/ar9001679
7. Wang, S.; Wang, X. *Appl. Catal., B* **2015,** *162,* 494–500. doi:10.1016/j.apcatb.2014.07.026
8. Inoue, T.; Fujishima, A.; Konishi, S.; Honda, K. *Nature* **1979,** *277,* 637–638. doi:10.1038/277637a0
9. Kato, H.; Kudo, A. *J. Phys. Chem. B* **2001,** *105,* 4285–4292. doi:10.1021/jp004386b
10. Kato, H.; Kudo, A. *Catal. Today* **2003,** *78,* 561–569. doi:10.1016/S0920-5861(02)00355-3
11. Kato, H.; Kudo, A. *Chem. Phys. Lett.* **1998,** *295,* 487–492. doi:10.1016/S0009-2614(98)01001-X
12. Kato, H.; Kobayashi, H.; Kudo, A. *J. Phys. Chem. B* **2002,** *106,* 12441–12447. doi:10.1021/jp025974n
13. Kato, H.; Kudo, A. *Chem. Lett.* **1999,** *28,* 1207–1208. doi:10.1246/cl.1999.1207
14. Kim, H. G.; Hwang, D. W.; Kim, J.; Kim, Y. G.; Lee, J. S. *Chem. Commun.* **1999,** *12,* 1077–1078. doi:10.1039/a902892g
15. Teramura, K.; Okuoka, S.-i.; Tsuneoka, H.; Shishido, T.; Tanaka, T. *Appl. Catal., B* **2010,** *96,* 565–568. doi:10.1016/j.apcatb.2010.03.021
16. Li, M.; Li, P.; Chang, K.; Wang, T.; Liu, L.; Kang, Q.; Ouyang, S.; Ye, J. *Chem. Commun.* **2015,** *51,* 7645–7648. doi:10.1039/C5CC01124H
17. Li, K.; Handoko, A. D.; Khraisheh, M.; Tang, J. *Nanoscale* **2014,** *6,* 9767–9773. doi:10.1039/C4NR01490A
18. Wang, Z.-Y.; Chou, H.-C.; Wu, J. C. S.; Tsai, D. P.; Mul, G. *Appl. Catal., A* **2010,** *380,* 172–177. doi:10.1016/j.apcata.2010.03.059
19. Tsai, C.-W.; Chen, H. M.; Liu, R.-S.; Asakura, K.; Chan, T.-S. *J. Phys. Chem. C* **2011,** *115,* 10180–10186. doi:10.1021/jp2020534
20. Wang, S.; Ding, Z.; Yao, W.; Lin, J.; Wang, X. *Angew. Chem., Int. Ed.* **2014,** *53,* 1034–1038. doi:10.1002/anie.201309426
21. Wang, S.; Ding, Z.; Wang, X. *Chem. Commun.* **2015,** *51,* 1517–1519. doi:10.1039/C4CC07225A

22. Liu, D.; Fernández, Y.; Ola, O.; Mackintosh, S.; Maroto-Valer, M.; Parlett, C. M. A.; Lee, A. F.; Wu, J. C. S. *Catal. Commun.* **2012**, *25*, 78–82. doi:10.1016/j.catcom.2012.03.025

23. Núñez, J.; de la Peña O'Shea, V. A.; Jana, P.; Coronado, J. M.; Serrano, D. P. *Catal. Today* **2013**, *209*, 21–27. doi:10.1016/j.cattod.2012.12.022

24. Wu, J.; Saito, M.; Takeuchi, M.; Watanabe, T. *Appl. Catal., A* **2001**, *218*, 235–240. doi:10.1016/S0926-860X(01)00650-0

25. Slamet; Nasution, H. W.; Purnama, E.; Riyani, K.; Gunlazuardi, J. *World Appl. Sci. J.* **2009**, *6*, 112–122.

26. Fujitani, T.; Nakamura, J. *Appl. Catal., A* **2000**, *191*, 111–129. doi:10.1016/S0926-860X(99)00313-0

27. Wang, S.; Hou, Y.; Wang, X. *ACS Appl. Mater. Interfaces* **2015**, *7*, 4327–4335. doi:10.1021/am508766s

28. Kaneco, S.; Shimizu, Y.; Ohta, K.; Mizuno, T. *J. Photochem. Photobiol., A: Chem.* **1998**, *115*, 223–226. doi:10.1016/S1010-6030(98)00274-3

29. Dey, G. R.; Belapurkar, A. D.; Kishore, K. *J. Photochem. Photobiol., A: Chem.* **2004**, *163*, 503–508. doi:10.1016/j.jphotochem.2004.01.022

30. Dey, G. R.; Pushpa, K. K. *Res. Chem. Intermed.* **2007**, *33*, 631–644. doi:10.1163/156856707781749883

31. Li, X.; Zang, J. *J. Phys. Chem. C* **2009**, *113*, 19411–19418. doi:10.1021/jp907334z

32. Xiong, P.; Tan, G.; Zhang, W.; Xia, A.; Ren, H. *J. Cluster Sci.* **2013**, *24*, 515–522. doi:10.1007/s10876-013-0557-4

33. Shi, J.; Liu, G.; Wang, N.; Li, C. *J. Mater. Chem.* **2012**, *22*, 18808–18813. doi:10.1039/c2jm33470d

34. He, Y.; Zhu, Y.; Wu, N. *J. Solid State Chem.* **2004**, *177*, 3868–3872. doi:10.1016/j.jssc.2004.07.011

35. Qin, S.; Xin, F.; Liu, Y.; Yin, X.; Ma, W. *J. Colloid Interface Sci.* **2011**, *356*, 257–261. doi:10.1016/j.jcis.2010.12.034

36. Liu, L.; Gao, F.; Zhao, H.; Li, Y. *Appl. Catal., B* **2013**, *134–135*, 349–358. doi:10.1016/j.apcatb.2013.01.040

37. Huang, L.; Peng, F.; Ohuchi, F. S. *Surf. Sci.* **2009**, *603*, 2825–2834. doi:10.1016/j.susc.2009.07.030

38. Li, G.; Dimitrijevic, N. M.; Chen, L.; Rajh, T.; Gray, K. A. *J. Phys. Chem. C* **2008**, *112*, 19040–19044. doi:10.1021/jp8068392

39. Colón, G.; Maicu, M.; Hidalgo, M. C.; Navío, J. A. *Appl. Catal., B* **2006**, *67*, 41–51. doi:10.1016/j.apcatb.2006.03.019

40. Liu, B.-J.; Torimoto, T.; Yoneyama, H. *J. Photochem. Photobiol., A* **1998**, *115*, 227–230. doi:10.1016/S1010-6030(98)00272-X

41. Kudo, A.; Miseki, Y. *Chem. Soc. Rev.* **2009**, *38*, 253–278. doi:10.1039/B800489G

42. Ganesh, I. *Renewable Sustainable Energy Rev.* **2014**, *31*, 221–257. doi:10.1016/j.rser.2013.11.045

43. Habisreutinger, S. N.; Schmidt-Mende, L.; Stolarczyk, J. K. *Angew. Chem., Int. Ed.* **2013**, *52*, 7372–7408. doi:10.1002/anie.201207199

44. Markiewicz, M. E. P.; Hebert, D. M.; Bergens, S. H. *J. Power Sources* **2006**, *161*, 761–767. doi:10.1016/j.jpowsour.2006.05.002

45. Mitoraj, D.; Kisch, H. *J. Phys. Chem. C* **2009**, *113*, 20890–20895. doi:10.1021/jp903893w

46. Dey, G. R. *J. Nat. Gas Chem.* **2007**, *16*, 217–226. doi:10.1016/S1003-9953(07)60052-8